A Time-Adjustable Model-Based Method for Fast State-of-Health Diagnosis of Lithium-Ion Batteries

Jérémy BLANC[c], Emmanuel SCHAEFFER[a], Raymonda DIAB[a,b,c], François AUGER[a], Jean-François COUSSEAU[c]

[a]Nantes Université, Institut de Recherche en Énergie Électrique de Nantes Atlantique, IREENA, UR 4642, F-44600 Saint-Nazaire, France

[b]Nantes Université, CNRS, Institut des Matériaux de Nantes Jean Rouxel, IMN, F-44000 Nantes, France

[c]One-sixone, F-44980 Sainte-Luce-sur-Loire, France

Reusing high-energy-density Li-ion batteries (LIBs) in less demanding applications can greatly reduce the environmental impact of electric vehicles. However, for battery reconditioning to be economically viable, it is crucial to accurately estimate the state of health (SoH) of each accumulator connected in series within the battery, at a lower cost. Traditional low-current or relaxation methods are unfortunately too time-consuming to meet the constraints of the reconditioning industry. This article presents a new model-based approach that allows the fast, time-adjustable estimation of the open-circuit voltage (OCV) to state-of-charge (SoC) relationship of Li-ion cells, as well as their incremental capacity (IC) curve. Indeed, tracking the peak amplitudes and positions of the IC-OCV curve provides information on their state of health and remaining useful life. The proposed method allows for obtaining a State of Health (SoH) estimation in just 2.5 hours with an accuracy of 2.7%.

Keywords–Li-ion batteries, Open circuit voltage, ICA-DVA, Second-life, Model-based diagnosis, LIB modeling, Extended Kalman filtering

1. INTRODUCTION

A battery consists of multiple Li-ion cells connected in series or parallel, depending on the voltage and current requirements of the system being powered. For several well-documented reasons, cells degrade at different rates, with the most degraded cell determining the overall capacity of the battery [1]. Consequently, a battery may reach the end of its useful life when only two or three cells have significantly deteriorated, while the remaining cells remain in excellent condition.

It is therefore easy to understand the importance of being able to accurately diagnose the state of health of all the cells in the battery, either to reuse the battery without dismantling it in a less demanding application, or to identify the few cells that need to be recycled and those that can be reused in reconditioned batteries. To do this, conventional diagnostic methods require the battery cells to be fully charged and discharged at very low current, which is time-consuming and impractical for large-scale battery evaluation [2].

However, some researchers have developed alternative methods like L. Vichard et al. [3] who present an online estimating method for SoC and SoH using a model approach and a Kalman filter. The model utilizes is a classic ECM with a complex expression of the OCV. The results are interesting, and the capacity-based SoH calculation uses the ratio between the variation of exchanged capacity and the variation of SoC. In [4] , X. Yu et al. propose a data-driven learning method to estimate the State of Health (SoH) and Remaining Useful Life (RUL) of batteries by analyzing online data received from the Battery Management System (BMS). They train their algorithm using datasets from NASA and CALCE, achieving promising results. However, while the majority of the literature focuses on SoH estimation of battery packs as a whole, rather than the SoH of individual cells within the pack, we propose a distinct approach to address this gap.

To deal with time constraints, we propose a model-based approach whose underlying principle is to estimate the voltage drop due to the different internal electrochemical phenomena (charge transfer, conduction, diffusion in solid and liquid phases) during the charging or discharging phases. Due to simplifying assumptions, the parameters values of the proposed equivalent circuit model are highly dependent on the state of charge, the temperature, and the current amplitude. And, their online estimation therefore requires superimposing to the more or less charging/discharging current a specific excitation optimized to sensitize all model parameters sufficiently and using efficient identification algorithms [5]. The following section presents the identification principle by a time-adjustable excitation protocol and the use of our original model to estimate the incremental capacity (IC) curve without derivation. Indeed, many recent works have shown that the amplitude and position of the IC curve can be related to the loss of cycling lithium and of active material [6, 7]. The next section presents the experiment conducted to prove the effectiveness of the proposed method. In particular, it is shown that the capacitance fading is clearly correlated with the amplitude of the characteristic IC peak, allowing for a significant reduction in the duration of experimental measurements needed to assess the battery's state of health.

2. METHODOLOGY

2.1. Local model of the LIB

The local behavior of the cell is illustrated by Figure 1 and modeled by a continuous-time state-space representation :

$$M(\boldsymbol{\theta}) \begin{cases} \dot{\mathbf{x}}(t,\boldsymbol{\theta}) = f(\boldsymbol{\theta}, \mathbf{x}(t,\boldsymbol{\theta}), \mathbf{u}(t)) \\ \mathbf{y}_m(t,\boldsymbol{\theta}) = g(\boldsymbol{\theta}, \mathbf{x}(t,\boldsymbol{\theta}), \mathbf{u}(t)) \end{cases} \tag{1}$$

where bold letters refer to vectors and $\mathbf{u}$, $\mathbf{y}_m$, $\mathbf{x}$, $\boldsymbol{\theta}$ denote the model input, output, state and unknown parameters, respectively. These vectors are defined are follow:

- the 2-dimensional input is $\mathbf{u}^t = [I_{\text{cell}}, Q_{\text{cell}}]$ with:

$$Q_{\text{cell}}(t_k) = Q_{\text{cell}}(0) + \int_0^{t_k} I_{\text{cell}}(t)\, dt \tag{2}$$

  where I_{cell} and Q_{cell} are the current and exchanged capacity of the cell;

- the 4-dimensional state vector is

$$\mathbf{x}^t = [V_{\text{oc}}, V_{\text{d1}}, V_{\text{d2}}, V_{\text{d3}}] \tag{3}$$

  where V_{oc} is the cell OCV and V_{di} are the voltage of the i^{th} RC cell of the foster structure modeling the diffusion phenomena in liquid and solid phases;

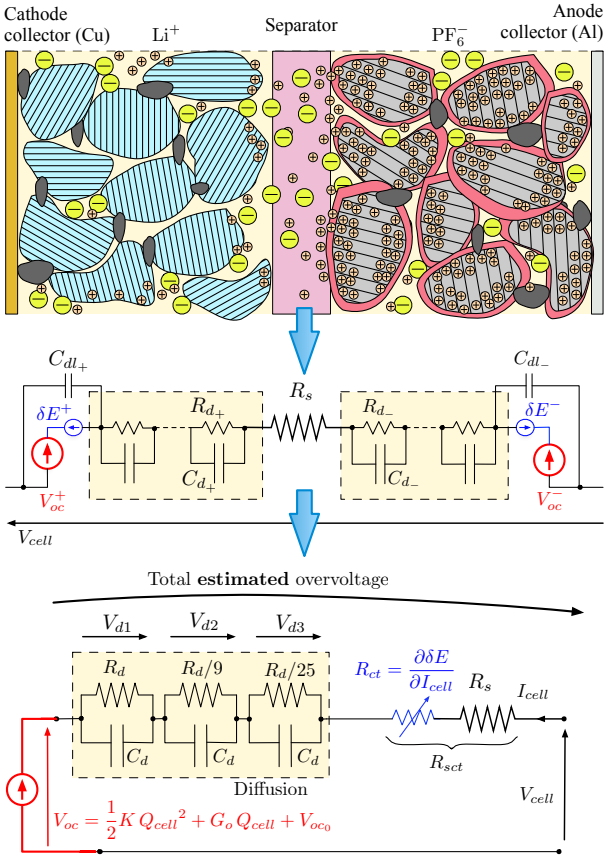

Figure 1. From a Pseudo 2D model to an equivalent circuit model of a Li-ion cell, by analogy between electrochemistry and electric circuit components. Since the model parameters (R_{stc}, R_d, C_d, Go, K) deal with first- or second-order approximations of physical phenomena, their values can only be considered constant for very small variations of current I_{cell}, temperature T and state-of-charge SoC.

- the 5-dimensional model parameters vector is chosen as:

$$\boldsymbol{\theta}^t = [R_{\rm sct}, G_o, K, G_{\rm d}, F_{\rm d}] \tag{4}$$

where $G_{\rm d} = 1/C_{\rm d}$ and $F_{\rm d} = 1/(R_{\rm d}\, C_{\rm d})$ characterize the dynamics of the diffusion phenomena which is discretized by a Foster struture of three components with resistance equal to $R_{\rm d}$, $R_{\rm d}/9$ and $R_{\rm d}/25$, the smallest time constant is equal to few seconds and is two time higher than time sampling in our method [8], whereas G_o and K relate the local variation of the OCV with respect to the SoC and R_{sct} characterize the ionic and electronic conduction as well as the charge transfert;

- the evolution equations are:

$$\begin{aligned}
\dot{x}_1(t,\boldsymbol{\theta}) &= \Big(G_o + K\, u_2(t)\Big)\, u_1(t) && (5)\\
\dot{x}_2(t,\boldsymbol{\theta}) &= -F_d\, x_2(t,\boldsymbol{\theta}) + G_d\, u_1(t) && (6)\\
\dot{x}_3(t,\boldsymbol{\theta}) &= -9\, F_d\, x_3(t,\boldsymbol{\theta}) + G_d\, u_1(t) && (7)\\
\dot{x}_4(t,\boldsymbol{\theta}) &= -25\, F_d\, x_4(t,\boldsymbol{\theta}) + G_d\, u_1(t) && (8)
\end{aligned}$$

- and the observation equation providing the simulated voltage:

$$y_m(t,\boldsymbol{\theta}) = \sum_{i=1}^{4} x_i(t,\boldsymbol{\theta}) + R_{stc}\, u_1(t) \tag{9}$$

2.2. *Excitation protocol*

The protocol is optimized by T and the principal time constant of the diffusion phenomena, which depends on the electrode chemistry of the tested cell and its power- or energy-oriented design [9]. To ensure the sensitivity of the model parameters sufficiently, the current excitation consists of the superposition of a constant current I and a periodic rectangular current of period τ_p, amplitude ΔI and duty cycle α (see Fig.2) where:

- The value of ΔI is tuned to be sufficiently large to ensure that the amplitude of the resulting voltage step response significantly exceeds the voltage resolution of the test bench. Concurrently, it is kept small enough to maintain the equivalent charge transfer resistance relatively constant. This resistance is fundamentally the inverse of the local derivative of the Butler-Volmer equation [10], which relates the current density to the electrode potential;

- the selection of τ_p and α is choosen to maximize the sensitivity of parameter vector.

Then, ΔI and α being defined, the constant current I required to respect the test duration is given by:

$$I = \frac{Q_{\rm nom}}{T} - \alpha\, \Delta I \tag{10}$$

and the number of square pulses (during the charge) is equal to T/τ_p. Finally, the time-adjustable protocol deals with the following algorithm:

- Step 0: Initially, the cell is fully charged and maintained at a constant maximum voltage until the current decreases below a specified threshold.

- Step 1: the cell is discharged using a periodic excitation current equal to $-I$ during $(1-\alpha)\,\tau_p$ and to $-(I+\Delta I)$ during $\alpha\tau_p$, the cell reaches the cut-off voltage. The voltage and current signals are sampled with a sampling period T_s that is boss less than 0.2 times the smallest time constant of the model and ensures that the voltage change between consecutive samples does not exceed 1.5 times the peak-to-peak measurement noise of the test bench. This approach enables accurate capture of the voltage step while minimising the data recording size.

- Step 2: the cell is charged using a periodic excitation current equal to I during $(1-\alpha)\,\tau_p$ and to $I+\Delta I$ during $\alpha\tau_p$ and acquired with the same sampling rule, until the charging cut-off voltage is reached.

The non-uniformly sampled record can subsequently be post-processed using an estimation algorithm EKF to provide estimated OCV values at each sample time.

2.3. *Continuous-discrete extented Kalman filter*

2.3.1. *Guideline principles*

For clarity, $\mathbf{v}_{[k]}$ and $\mathcal{M}_{[k]}$ denotes the values of the vector $\mathbf{v}$ and the matrix $\mathcal{M}$ at time t_k, respectively. The CDEKF [11] is an identification algorithm derived from a continuous-time dynamic model and a discrete-time measurements of the system output. It estimates both the model states and parameters which are assumed to be constant or randomly varying, using an augmented state vector $\mathbf{x}_a = [\mathbf{x}; \boldsymbol{\theta}]$ with $\dot{\boldsymbol{\theta}} = 0$. The CDEKF algorithm [12, 13] consists of a two-phase process:

- a continuous-time **prediction** of the augmented state $\mathbf{x}_{a\,[k+1]}^{p}$ and of the prediction error covariance matrix $\mathcal{P}_{[k+1]}^{p}$ is achieved through the numerical integration of

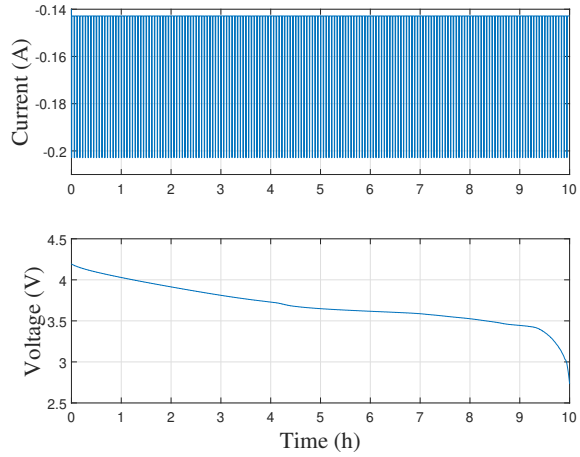

(a) Current and voltage used by the MHE and EKF identification algorithms.

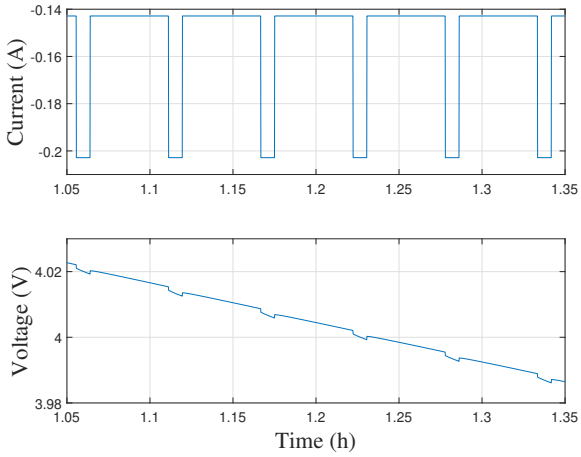

(b) Zoom on the excitation current wave and the resulting voltage response.

Figure 2. Protocol during the discharge phase dedicated to the OCV estimation by our model-based method, with $\Delta I = 60$ mA, $\tau_p = 200$ s, $\mu_c = 0.15$ and $T = 10$ h.

the following two Ordinary Differential Equations over the interval from t_k to t_{k+1}:

$$\dot{\mathbf{x}}_a^p(t) = f_a\left(\mathbf{x}_a^p(t), \mathbf{u}(t)\right) \quad (11)$$

$$\dot{\mathcal{P}}_p(t) = \mathcal{F}(t)\,\mathcal{P}^p(t) + \mathcal{P}^p(t)\,\mathcal{F}(t)^t + \mathcal{Q} \quad (12)$$

$$\text{with } \mathcal{F}(t) = \frac{\partial f_a}{\partial \mathbf{x}_a}\left(\mathbf{x}_a^p(t), \mathbf{u}(t)\right) \quad (13)$$

with $f_a(\mathbf{x}_a, \mathbf{u}) = [f(\boldsymbol{\theta}, \mathbf{x}, \mathbf{u}); \mathbf{0}]$, and using $\mathbf{x}_a^p(t_k) = \mathbf{x}_a^e[k]$ and $\mathcal{P}^p(t_k) = \mathcal{P}^e[k]$ as initial values and $\mathbf{u}[k]$ as $\mathbf{u}(t)$. $\mathcal{Q}$ is a covariance matrix evaluating the model inaccuracy. Eq. 11 can be efficiently solved using implicit Runge-Kutta algorithms [14], whereas Eq. 12 can be efficiently solved using Mazzoni's formulas [15, 16];

- a discrete-time **update** of the augmented state estimate $\mathbf{x}_a^e[k+1]$ and its estimation error covariance matrix $\mathcal{P}^e[k+1]$ is performed using the predictions $\mathbf{x}_a^p[k+1]$ and $\mathcal{P}^p[k+1]$, along with the present measurement $\mathbf{y_s}[k+1]$ of the system output:

$$\begin{aligned}\mathbf{x}_a^e[k+1] = \mathbf{x}_a^p[k+1] + \mathcal{K}[k+1] \\ \left(\mathbf{y_s}[k+1] - \mathbf{g}_a\left(\mathbf{x}_a^p[k+1], \mathbf{u}[k]\right)\right)\end{aligned} \quad (14)$$

$$\mathcal{P}^e[k+1] = \mathcal{P}^p[k+1] - \mathcal{K}[k+1]\mathcal{G}[k+1]\mathcal{P}^p[k+1] \quad (15)$$

with $\mathbf{g}_a\left(\mathbf{x}_a, \mathbf{u}\right) = \mathbf{g}\left(\boldsymbol{\theta}, \mathbf{x}, \mathbf{u}\right)$ and

$$\mathcal{G}[k+1] = \frac{\partial g_a}{\partial \mathbf{x}_a}(\mathbf{x}_a^p[k+1], \mathbf{u}[k]) \quad (16)$$

$$\mathcal{K}[k+1] = \mathcal{P}^p[k+1]\;\mathcal{G}[k+1]^t\;\;\mathcal{S}[k+1]^{-1} \quad (17)$$

$$\mathcal{S}[k+1] = \mathcal{G}[k+1]\;\mathcal{P}^p[k+1]\;\mathcal{G}[k+1]^t + \mathcal{R} \quad (18)$$

where $\mathcal{R}$ is a covariance matrix evaluating the sensor noise.

In this context, $\mathbf{y_s}[k]$ represents a one-dimensional signal. It has been demonstrated [17] that $\mathcal{R}$ can be set to 1. The CDEKF algorithm is set by the three matrices $\mathcal{Q}$, $\mathbf{x}_a^e[0]$ and $\mathcal{P}^e[0]$. Once appropriately tuned, the CDEKF algorithm, when applied to the proposed model, provides an estimation of the OCV and its uncertainty (represented by the first diagonal element of the estimation error covariance matrix $\mathcal{P}^e[k]$) at each time t_k. Given the cell capacitance Q_{nom}, this allows for the construction of the OCV-SoC curve with a high density of points, as well as the ICA or DVA indicators.

2.3.2. *Nonlinear observability of the model*

Let's recall that a sufficient local observability condition [18] of a non-linear n-order model $M : \begin{cases} \dot{\mathbf{x}} = f(\mathbf{x}, \mathbf{u}) \\ y = g(\mathbf{x}, \mathbf{u}) \end{cases}$ at point $\mathbf{x}_o$ is that there exists an entry and its $n-1$ first time derivatives $\{\mathbf{u}, d\mathbf{u}/dt, d^2\mathbf{u}/dt^2, \ldots\}$ such as the rank of the Jacobian matrix

$$J(\mathbf{x}_o) = \left[\frac{\partial}{\partial \mathbf{x}}\begin{pmatrix} g(\mathbf{x}, \mathbf{u}) \\ (L_f g)(\mathbf{x}, \mathbf{u}) \\ \vdots \\ (L_f^{n-1} g)(\mathbf{x}, \mathbf{u}) \end{pmatrix}|_{\mathbf{x}=\mathbf{x}_o}\right] \quad (19)$$

is full, the Lie operator L_f being defined by [19]:

$$L_f g(\mathbf{x}, \mathbf{u}) = \left[\frac{\partial g(\mathbf{x}, \mathbf{u})}{\partial \mathbf{x}}\right] f(\mathbf{x}, \mathbf{u}) + \left[\frac{\partial g(\mathbf{x}, \mathbf{u})}{\partial \mathbf{u}}\right] \frac{d\mathbf{u}}{dt} \quad (20)$$

To ensure the estimability of the model parameters using an EKF, the observability of the extended state-space model, defined by the state equation (Eq. 11) and the observation equation (Eq. 9) can be analyzed. The classical approach involves determining the conditions under which the determinant of the Jacobian matrix does not vanish. Due to the complex analytical expression of the Jacobian matrix, this analysis is conducted using a computer algebra system. It was determined that local observability depends on the state variables and the input current protocol. For an input signal defined as $u_1(t) = 0.6 + 0.03\sin(\omega\, t)$ which approximates the excitation protocol, local observability is guaranteed if the parameter F_d is non-zero, which is inherently the case. Since the actual excitation protocol can be expanded into a Fourier series, i.e. a sum of an infinite number of sinusoids, the real system input is even more persistently exciting than the above sum of one constant and one sinusoid. And thus one can reasonably consider that the system is locally observable.

2.4. *Estimation of the incremental capacity*

At each $SoC(t)$, the IC can be obtained by:

$$IC = \frac{\partial V_{oc}}{\partial Q}(t, \theta) = \frac{\frac{\partial V_{oc}}{\partial t}(t, \theta)}{\frac{\partial Q}{\partial t}(t)} = (G_o + K\, u_2(t)) \quad (21)$$

Our model enables direct access to the IC indicator without the need to derive it from the cell's OCV by the exchanged cell capacity Q. This approach avoids potential information loss and noise generation associated with this process.

3. EXPERIMENTS AND DISCUSSIONS

3.1. Tested Li-ion cells

To validate the proposed method, we use three different Li-ion cells. Their specifications are detailed in Table 1.

3.2. IC-OCV curve estimation

Figures 3 to 5 compare the IC-OCV curve otained by our method (EKF) with ones obtained by a classical (LC) tests at $C/25$ C-rate. We observe an accurate estimation of the IC-OCV curve for two NMC cells by the proposed method. For the LFP cell, the estimation is correct, but presents difficulty in dissociating the two peaks due to a change of lithium insertion stage in the negative electrod; we estimate only a principal peak which covers the two peaks. We can use this IC-OCV curve estimation to estimate Li-ion cell SoH.

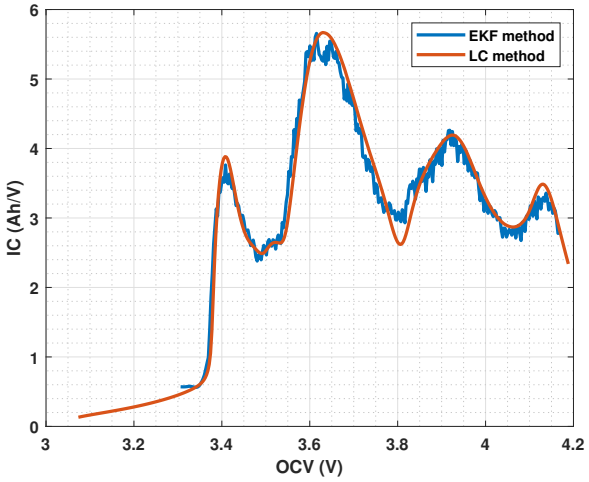

Figure 3. IC-OCV curve comparison of Cell 1.

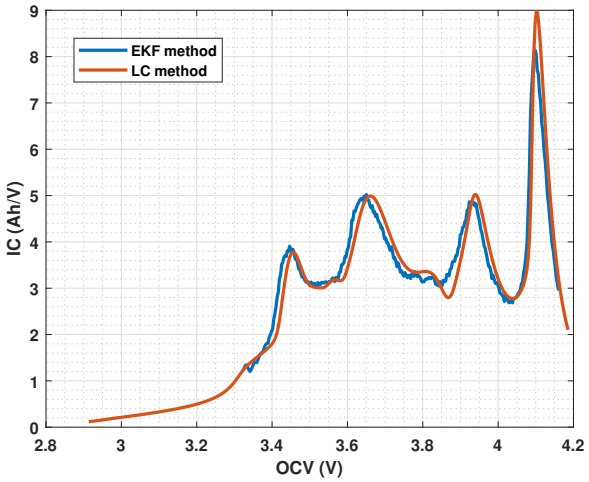

Figure 4. IC-OCV curve comparison of Cell 2.

3.3. SoH estimation

For each Li-ion cell reference, we take nine samples and age them at different stages. Their IC curves are derived from the cell identification as detailed in section 2, and their remaining capacity is measured by a standard industrial protocol.

Figures 6 to 8 exhibit accurate results for each Li-ion cell reference with a relative error of less than 2.8%. Moreover, using

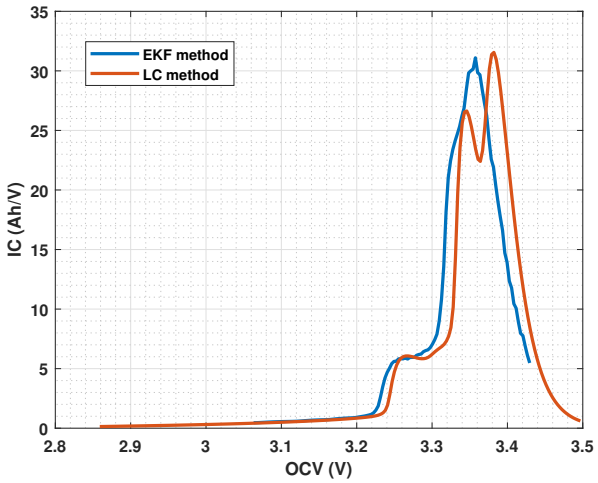

Figure 5. IC-OCV curve comparison of Cell 3.

the least squares approach, we show the linear relationship between the estimated IC peak amplitudes H_{mp} obtained with the characterization protocol of 10 hours and the measured cell capacity (in accordance with previous work [20]):

$$Q_{cell} = a\, H_{mp} + b \tag{22}$$

Table 2 summarizes the parameters of linear regression for Li-ion cells tested and their accuracy. This method is accurate for each reference tested with RMS error less than 1.02% and maximum error less than 2.69%.

$$\text{RMS error} = \sqrt{\frac{1}{N}\sum_{n=0}^{N-1}\left(\widehat{\text{SoH}} - \text{SoH}^{\text{ref}}\right)^2} \tag{23}$$

where N is the number of characterization points of SoH obtained by the reference method, $\widehat{\text{SoH}}$ are the SoH estimated by the proposed method and SoH^{ref} are the SoH values provided by the reference method.

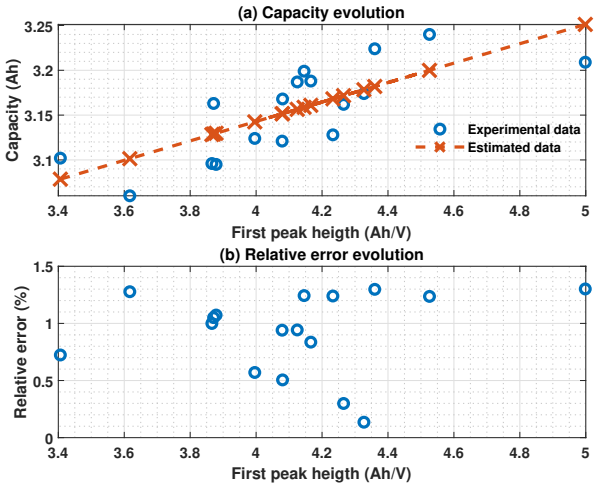

Figure 6. SoH estimation by linear regression of Cell 1.

3.4. Time constraint of the proposed method

To test the limit of the proposed method, we set the protocol according to section 2.2 with I equal to $C/5$ and $C/3$. For the cell reference 1 and 2 we apply the protocol between 0 and 30%

	Cell 1	Cell 2	Cell 3
Reference	Panasonic NCR 18650B	Samsung INR1865035E	PLB IFR266533A
Chemistry	NMC	NMC	LFP
Capacity (Ah)	3.35	3.45	3.3
Format	Cylindrical	Cylindrical	Cylindrical
Dimension	18650	18650	26650
Min Voltage cutoff (V)	2.5	2.5	2
Max Voltage cutoff (V)	4.2	4.2	3.65
Max charge current (A)	6.7	8.0	9.9
Max discharge current (A)	10	13	16.5
Weigth (g)	48	50	88

Table 1. Technical informations about tested cells for experiments.

	Cell 1	Cell 2	Cell 3
a (V)	0.108	0.9292	0.028
b (Ah)	2.709	-0.048	2.310
RMS error (%)	0.99	0.96	1.02
Max error (%)	1.30	2.69	2.32

Table 2. Technical informations about tested cells for experiments.

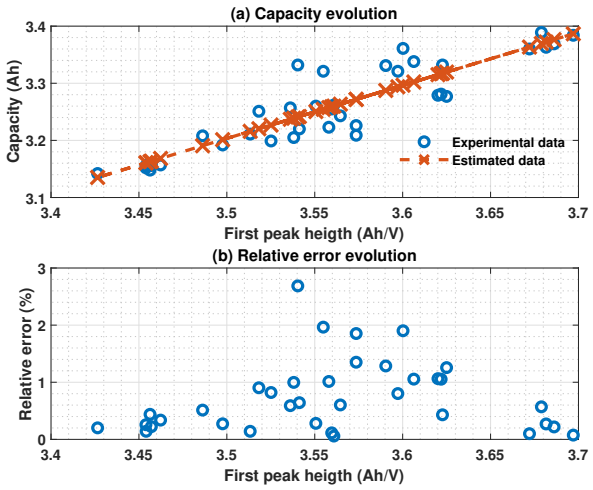

Figure 7. SoH estimation by linear regression of Cell 2.

of SoC and the cell reference 3 between 10 and 90% of SoC which deals with SoC range Where IC is pretty sensitive to SoH (see Fig 3 to 5). Two samples of each reference cell are used and we compare the SoH identified with the proposed method to the SoH estimate with a reference method.

Fig 9 shows the SoH estimation obtained by the proposed method, we observe an error less than 2.2% with a current at $C/5$ and 2.7% at $C/3$. The results are accurate and demonstrate the possibility to estimate the SoH in only 1 hour at $C/3$ or 1 hour and half at $C/5$ for the reference cell 1 and 2 and in only 2 hours and half at $C/3$ or 4 hours at $C/5$ for reference cell 3.

4. CONCLUSIONS

To conclude, the use of the IC-OCV curve is a key tool to estimate accurately and rapidly the SoH of Li-ion cells, especially in a pack configuration where it is impossible to charge and discharge fully each cell as recommended with reference methods. The proposed method is based on a model and EKF algorithm to estimate online and accurately the OCV and on a tunable protocol to adapt the time protocol to the time constraints. The results demonstrate the possibility to estimate the SoH in only 1 hour

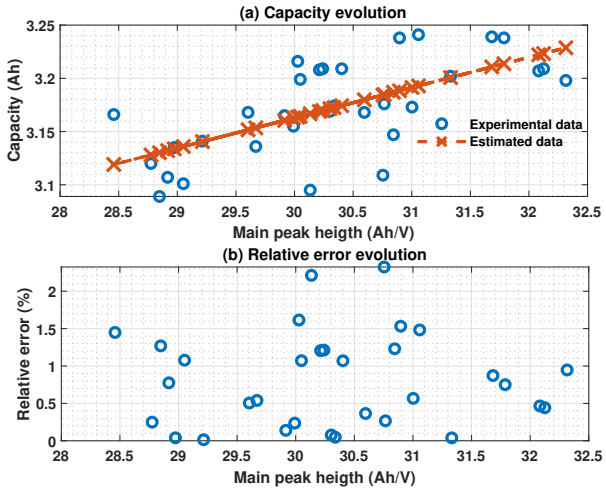

Figure 8. SoH estimation by linear regression of Cell 3.

at $C/3$ or 1 hour and half at $C/5$ for the NMC cell and in only 2 hours and half at $C/3$ or 4 hours at $C/5$ for LFP cell. To improve our method, it will be interesting to couple our method with a model of OCP superposition to estimate precisely the location of the degradation and predict the remain usefull life.

5. REFERENCES

[1] M. Broussely and Ph. Biensan and F. Bonhomme and Ph. Blanchard and S. Herreyre and K. Nechev and R.J. Staniewicz c, « Main aging mechanisms in Li ion batteries », Journal of Power Sources, Vol 146, 2005.

[2] S. Vignesh and H. S. Che and J. Selvaraj and K. S. Tey and J. W.Lee and H. Shareef and R. Errouissi, « State of Health (SoH) estimation methods for second life lithium-ion battery—Review and challenges », Applied Energy, Vol 369, 2024.

[3] L. Vichard and A. Ravey and P. Venet and F. Harel and S. Pelissier and D. Hissel, « A method to estimate battery SOH indicators based on vehicle operating data only », Energy, Vol 225, 2021.

[4] X. Yu and Z. Ma and J. Wen, « Joint estimation of SOH and RUL for lithium batteries based on variable frequency and model integration », International Journal of Electrochemical Science, 2024.

[5] J. Blanc, E. Schaeffer, F. Auger, Y. Diab, and J. F. Cousseau, « A new time-adjustable model-based method for fast open-circuit voltage estimation of Lithium-ion cells », Journal of Power Sources, VOL. 586, Dec 2023

[6] M. Dubarry, C. Truchot and B. Y. Liaw, « Synthesize battery degradation modes via a diagnostic and prognostic model », Journal of Power Sources, Vol 219, p. 204-216 2012.

[7] D. Ansean, V. M. Garcia, M. Gonzalez, C. Blanco-Viejo, J. C. Viera, Y. F. Pulido, and L. Sanchez, « Lithium-Ion Battery Degradation Indicators Via Incremental Capacity Analysis », IEEE Transactions on industry application, Vol 55 No 3, 2019.

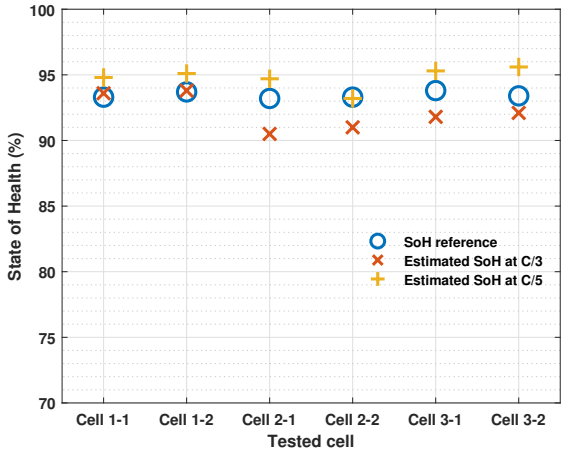

Figure 9. Time performance of the proposed method to estimate SoH for three Li-ion cells reference.

[8] E. Kuhn, C. Forgez, P. Lagonotte and G. Friedrich, “Modelling Ni-mH battery using Cauer and Foster structures”, Journal of Power Sources, Vol. 158.2, pp. 1490-1497, (2006).

[9] Han Gao, Qiang Wu, Yixin Hu, Jim P. Zheng, Khalil Amine, and Zonghai Chen, “Revealing the Rate-Limiting Li-Ion Diffusion Pathway in Ultrathick Electrodes for Li-Ion Batteries", The Journal of Physical Chemistry Letters, Vol 9, pp 5100-5104, (2018).

[10] Edmund J.F Dickinson, and Andrew J. Wain, “The Butler-Volmer equation in electrochemical theory: Origins, value, and practical application" Journal of Electroanalytical Chemistry, 114145, 872, (2020).

[11] J. B. Jørgensen, “A critical discussion of the continuous-discrete extended Kalman filter,”

[12] I. Hwang, H. Balakrishnan, and C. Tomlin, “State estimation for hybrid systems: applications to aircraft tracking”, IEE Proceedings - Control Theory and Applications, Vol. 153, No. 5, pp. 556–566, (2006).

[13] Yasser Diab, François Auger, Emmanuel Schaeffer and Moutassem Wahbeh, “Estimating Lithium-Ion Battery State of Charge and Parameters Using a Continuous-Discrete Extended Kalman Filter", MPDI energies, Vol 10, (2017).

[14] J.-M. Guihal, F. Auger, N. Bernard and E. Schaeffer, “Efficient Implementation of Continuous-Discrete Extended Kalman Filters for State and Parameter Estimation of Nonlinear Dynamic Systems", IEEE Trans. on Industrial Informatics, Vol. 18, No. 5, pp. 3077-3085, (2022).

[15] T. Mazzoni, “Computational aspects of continuous-discrete extended Kalman-filtering,” Computational Statistics, Vol. 23, No. 4, pp. 519–539, (2008).

[16] Y. Diab, F. Auger, E. Schaeffer, S. Chevalier, A. Allahham, “Real-Time Estimation of PEMFC Parameters Using a Continuous-Discrete Extended Kalman Filter Derived from a Pseudo-Two-Dimensional Model", Energies, Vol 15, 2337, (2022).

[17] Sergio Bittanti, Sergio M. Savaresi, “On the parametrization and design of an extended Kalman filter frequency tracker”, IEEE Trans. Autom. Control, Vol. 45, No. 9, pp. 1718–1724 (2000).

[18] R. Hermann and A. Krener, "Nonlinear controllability and observability", IEEE Trans. on Aut. Cont., Vol. 22, No. 5, pp. 728 - 740, (1977).

[19] R. L. Spyker and R. M. Nelms, "Classical equivalent circuit parameters for a double layer capacitor", IEEE Trans. on Aero. and Ele. Sys., Vol. 36, No. 3, pp. 829 - 836, (2000).

[20] J. He, Z. Wei, Y. Hu, X. Bian, and F. Yan, « State-of-Health Estimation of Lithium-Ion Batteries Using Incremental Capacity Analysis Based on Voltage–Capacity Model », IEEE Transactions on transportation electrification, VOL. 6, NO. 2, p. 417-425, June 2020